



# Preparation and nitrogen-doping of three-dimensionally ordered macroporous TiO<sub>2</sub> with enhanced photocatalytic activity

Yan Dong<sup>a</sup>, Youhe Wang<sup>a,b,\*</sup>, Tonghui Cai<sup>a</sup>, Long Kou<sup>a</sup>, Guidong Yang<sup>c</sup>, Zifeng Yan<sup>a,\*\*</sup>

<sup>a</sup>State Key Laboratory for Heavy Oil Processing, Key Laboratory of Catalysis, CNPC, China University of Petroleum, Qingdao 266555, China

<sup>b</sup>School of Science, China University of Petroleum, Qingdao 266555, China

<sup>c</sup>Department of Chemical Engineering, School of Chemical Engineering and Technology, Xi'an Jiaotong University, Xi'an 710049, China

Received 7 February 2014; received in revised form 27 March 2014; accepted 27 March 2014

## Abstract

Three-dimensionally ordered macroporous titanium dioxide (3DOM TiO<sub>2</sub>) was synthesized through a colloidal crystal template method using self-made poly-(methyl methacrylate) (PMMA) microspheres as a hard template. Nitrogen-doped 3DOM TiO<sub>2</sub> (N-3DOM TiO<sub>2</sub>) samples were also prepared by an impregnation method. The samples were characterized by techniques such as SEM, EDX, XRD, TGA, and UV–visible spectroscopy. The photocatalytic activities of these catalysts were tested by degradation of methyl orange (MO) under UV–visible light and visible light respectively. The experimental results show that the 3DOM TiO<sub>2</sub> and N-3DOM TiO<sub>2</sub> exhibited improved optical absorption and subsequently enhanced photodegradation efficiency of MO compared to TiO<sub>2</sub> particles.

© 2014 Elsevier Ltd and Techna Group S.r.l. All rights reserved.

**Keywords:** B. Porosity; D. TiO<sub>2</sub>; Nitrogen doping

## 1. Introduction

In recent years, three-dimensionally ordered macroporous (3DOM) materials have been attracting considerable attention due to their great potentials in a variety of areas including catalysis [1], adsorption [2], gas sensing [3], supercapacitor electrodes [4], and photonic crystals [5]. The unique 3DOM structure can provide interconnectivity among the porous network, which can increase diffusion rates of reactant molecules and make the active sites more accessible [6]. Furthermore, 3DOM structures have also been recognized as a photonic crystal which can enhance the light absorption of material and improve its photoreaction efficiency due to the

structure-induced generation of slow photons [7,8]. Considering the great application and commercial value of 3DOM material, great efforts have been devoted to fabricate and characterize 3DOM materials [9]. Up to date, a large number of 3DOM materials have been prepared by a variety of synthesis methods. The colloidal crystal template method is considered as an effective yet simple strategy for the production of 3DOM materials. In this method, a colloidal crystal template is initially prepared by ordering monodisperse spheres consisting of poly-(methyl methacrylate) (PMMA), polystyrene (PS), or silica. The resulting colloidal crystal template is then immersed into the fluid precursor. During this process, the precursor molecules infiltrate into the interstices between ordered spheres and then hydrolyze and precipitate, forming an intermediate composite structure. The template spheres are then removed by calcination or extraction, leaving an inverse opal replica of the array of ordered spheres [5,6].

More recently, a variety of 3DOM metal oxides such as TiO<sub>2</sub> [10], ZrO<sub>2</sub> [11], SiO<sub>2</sub> [12] and Al<sub>2</sub>O<sub>3</sub> [13] were synthesized based on the colloidal crystal template method.

\*Corresponding author at: China University of Petroleum, State Key Laboratory for Heavy Oil Processing, Key Laboratory of Catalysis, CNPC, No. 66, Changjiang West Road, Qingdao 266555, China.  
Tel.: +86 532 86981856.

\*\*Corresponding author. Tel.: +86 532 86981296; fax: +86 532 86981295.  
E-mail addresses: [yhewang0168@gmail.com](mailto:yhewang0168@gmail.com) (Y. Wang),  
[zfyancat@upc.edu.cn](mailto:zfyancat@upc.edu.cn) (Z. Yan).

Among them,  $\text{TiO}_2$ , a common photocatalyst which is widely used in the area of solar energy conversion [14,15] and environmental purification [16,17], was intensively studied for its high photoactivity, good chemical stability, nontoxicity and low cost [18]. Compared to traditional  $\text{TiO}_2$  nanoparticles, 3DOM  $\text{TiO}_2$  catalyst possesses not only better mass transfer properties but also higher light absorption efficiency owing to the structure induced multiple scattering and slow photons generated near the edges of its photonic gap [7] resulting in higher photocatalytic activity [8]. However, a major barrier to the widespread use of 3DOM  $\text{TiO}_2$  is its large electronic energy gap (3.2 eV). Such gap practically limits its excitation with the ultraviolet (UV) part of the solar irradiation. This is challenging because UV light accounts for only 4% of the incoming solar energy [19]. Therefore it is important to widen the absorption spectrum of  $\text{TiO}_2$  to develop more efficient solar energy devices and develop higher-efficiency photocatalysts. Progress has been made by doping  $\text{TiO}_2$  with nonmetallic elements including nitrogen [20,21], sulfur [22], carbon [23] and fluorine [24,25]. Such strategy has resulted in a shift in the optical absorption edge of  $\text{TiO}_2$  toward lower energy, resulting in increased photocatalytic activity by visible light.

In this work, we describe a facile method to synthesize 3DOM  $\text{TiO}_2$  through the colloidal crystal template method with self-made PMMA as a hard template. Then an impregnation method with urea as the nitrogen source was introduced to modify the as-prepared 3DOM  $\text{TiO}_2$  to obtain N-3DOM  $\text{TiO}_2$ . Photocatalytic activity of the 3DOM  $\text{TiO}_2$  and N-3DOM  $\text{TiO}_2$  was evaluated by the photodegradation of methyl orange (MO) under UV–visible light and visible light respectively. Both N-3DOM  $\text{TiO}_2$  and 3DOM  $\text{TiO}_2$  show significantly higher photocatalytic efficiency compared to pure  $\text{TiO}_2$  particles that were used as the benchmark.

## 2. Reagents and methods

### 2.1. Chemicals

Methyl methacrylate (C98%), urea (C99%) and tetrabutyl titanate (C98%) were purchased from Sinopharm Chemical Reagent Co. Ltd. Potassium persulfate (C99%) was bought from Aijianxiancheng Reagent Co. Titanium isopropoxide (C98%) was acquired from Acros Organics. Ethanol (C99.7%) and hydrochloric acid (C36–38%) were purchased from Xilong Chemical Co. Ltd.

### 2.2. Synthesis of 3DOM $\text{TiO}_2$ and N-3DOM $\text{TiO}_2$

3DOM  $\text{TiO}_2$  was synthesized by the colloidal crystal template method. 3 g of titanium isopropoxide was dissolved in 6 g of ethanol in a beaker. 3 g of PMMA, which was synthesized using a previously developed method [13], was then immersed into the solution. The beaker was placed in a hot water bath for 24 h at 40 °C. Finally, the white monolith was calcined in a muffle furnace at 500 °C for 5 h with a heating rate of 1 °C/min. Meanwhile,  $\text{TiO}_2$

particles (NP  $\text{TiO}_2$ ), which were used as a benchmark to evaluate 3DOM  $\text{TiO}_2$  and N-3DOM  $\text{TiO}_2$  photocatalytic activity, were prepared by sol–gel method: 20 ml tetrabutyl titanate was dissolved in 30 ml absolute ethanol to form solution A meanwhile 3 ml hydrochloric acid (C36–38%) was dissolved in 10 ml pure water to form solution B. Then, solution B was added into solution A dropwise under furious stir. After stirred for another hour, the mixture was transferred and kept in a hot water bath at 30 °C for 24 h to get the light yellow gel, which was then dried at 80 °C for 24 h. After drying, the gel turned to yellow monoliths which were then milled into powder in an agate mortar. Finally, the powder was calcined in a muffle furnace at 450 °C for 5 h at a ramping rate of 5 °C/min to get NP  $\text{TiO}_2$ .

A simple impregnation method was adopted to synthesize N-3DOM  $\text{TiO}_2$  and nitrogen-doped NP  $\text{TiO}_2$  (N-NP  $\text{TiO}_2$ ). 4 g 3DOM  $\text{TiO}_2$  or 4 g NP  $\text{TiO}_2$  as described above was soaked in 40 ml of a 4 M urea aqueous solution in a beaker. The beaker was placed in a hot water bath for 4 h at 40 °C. Then the excess urea solution was removed from the impregnated 3DOM  $\text{TiO}_2$  or NP  $\text{TiO}_2$  by vacuum filtration. The resulting monoliths or powder were calcined in a muffle furnace. To get N-3DOM  $\text{TiO}_2$ , the obtained monoliths (as-made N-3DOM  $\text{TiO}_2$ ) were calcined at 500 °C for 5 h at a ramping rate of 1 °C/min. To get N-NP  $\text{TiO}_2$ , the obtained powder (as-made N-NP  $\text{TiO}_2$ ) was calcined at 450 °C for 5 h at a ramping rate of 5 °C/min.

### 2.3. Characterization

Powder X-ray diffraction (XRD) was conducted using a PANalytical X'Pert PRO diffractometer with  $\text{CuK}\alpha$  radiation and a Ni filter in the range  $2\theta=5\text{--}75^\circ$ . Thermal gravimetric (TG) analysis was performed in an air flow of 100 ml/min at a ramping rate of 1 °C/min on a Linseis STA PT1600 instrument. Scanning electron microscopy (SEM) images were acquired with a HITACHI S-4800 operating at 3.0–5.0 kV. Energy dispersive X-ray spectrum (EDX) was obtained with an S-4800 high resolution analytical field emission SEM operating at 20.0 kV. The UV–visible absorption spectrum of the  $\text{TiO}_2$  samples was observed with an Analytikjena SPECORD 205 operating at a scanning range of 200 to 1100 nm.

### 2.4. Photocatalytic testing

The photocatalytic performance of 3DOM  $\text{TiO}_2$  and N-3DOM  $\text{TiO}_2$  was evaluated through degradation of MO using a 300 W Xe arc lamp (PLS-SXE300/300UV) with emission wavelength range from 110 nm to 1000 nm. For visible light measurements, a 400 nm cut-off glass filter was mounted before the output of light source to remove UV light and admit only visible light to enter into the reactor. For these MO degradation tests, 0.06 g of the three  $\text{TiO}_2$  based samples were each dispersed in 30 ml aqueous MO solutions containing 4 mg MO/L. The dispersions were kept in the dark for 0.5 h with magnetic stir to achieve equilibrium. An aliquot of 3.0 ml was collected every 10 min after initiation of the degradation tests. All aliquots were centrifuged at 10,000 rpm for 3 min to fully separate the catalyst from the solution.

The concentration of the residual MO was analyzed by UV–visible absorption at 463 nm.

### 3. Results and discussion

#### 3.1. Catalyst characterization

Fig. 1A shows the SEM image of the resulting PMMA colloidal crystal template. The closely packed PMMA microspheres exhibited uniformity in diameter of 240 nm and periodicity. In addition, a color change can be clearly observed when changing the viewing angle of the sample; this can be explained by the Bragg diffraction of the PMMA colloidal crystal template indicating the good uniformity and periodicity

of the template. Fig. 1B and C shows SEM images of the calcined 3DOM TiO<sub>2</sub>. A highly ordered macroporous structure is observed, while the dark areas of the structure indicate the air spheres and the lighter areas indicate the pore walls. The air spheres are well-ordered and connected by the holes on the pore wall, creating a three-dimensionally ordered macroporous structure. In addition, a multi-layer porous structure can be clearly seen in Fig. 1C, which is further proof of the existence of 3DOM structure. The pore diameter of the macropores is 160 nm, exhibiting a 33% contraction compared to the diameter of the PMMA microspheres. This is explained by the shrinking of the PMMA microspheres during the calcination process. In addition, similar shrinking was observed during the synthesis of 3DOM Al<sub>2</sub>O<sub>3</sub>, SiO<sub>2</sub> and ZrO<sub>2</sub> using the similar synthesis strategy [27,28], and the percent shrinkage of these 3DOM oxides was 26–34%, which is consistent

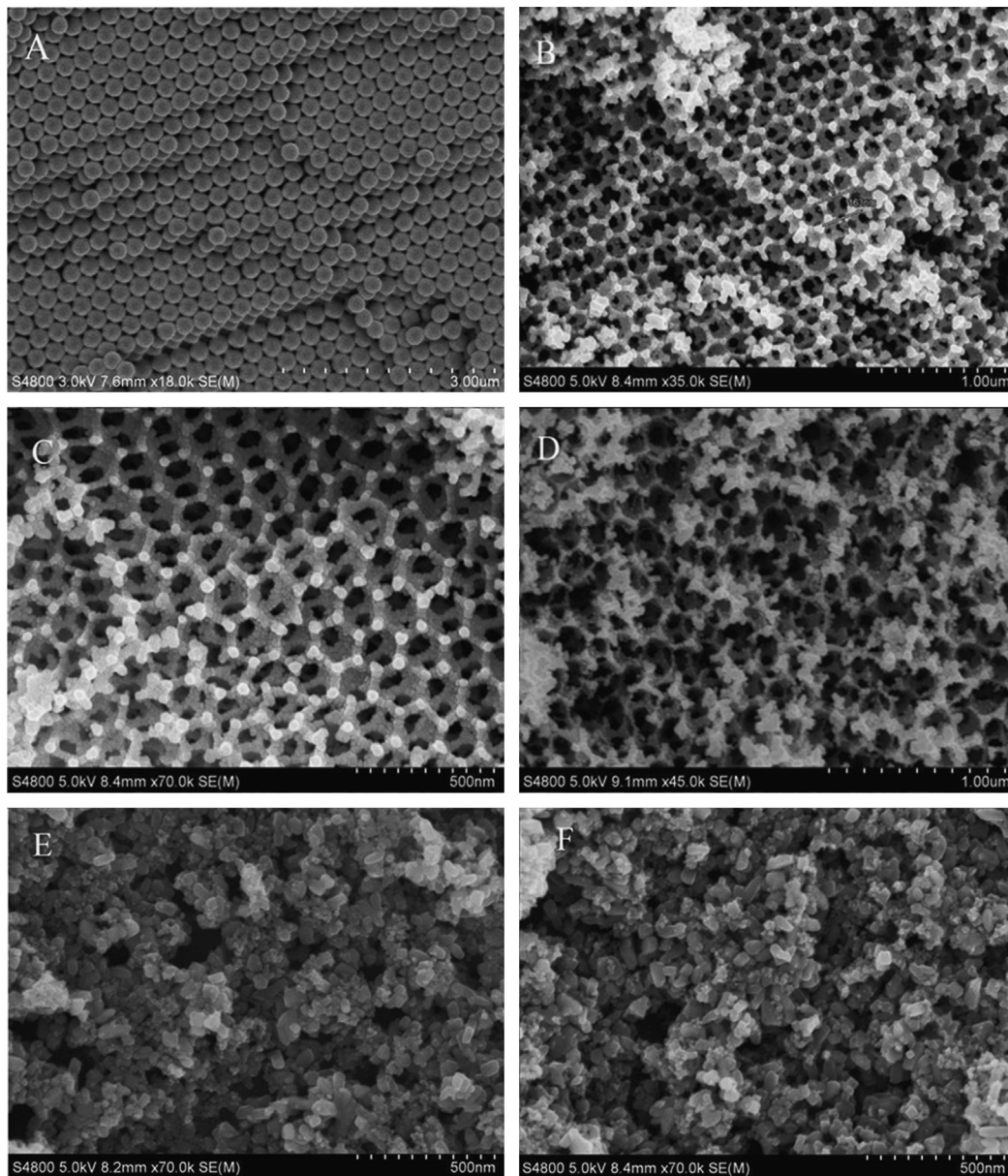


Fig. 1. SEM images of (A) PMMA colloidal crystal template; (B, C) 3DOM TiO<sub>2</sub>; (D) N-3DOM TiO<sub>2</sub>; (E) NP TiO<sub>2</sub> and (F) N-NP TiO<sub>2</sub>.

with the 33% contraction of the 3DOM TiO<sub>2</sub>. Despite shrinkage and a few local collapses (non-uniform white images shown in Fig. 1B and C), the well-structured 3DOM framework was retained after calcination, indicating good thermal stability of the samples. Fig. 1D shows the morphology of N-3DOM TiO<sub>2</sub>. Select breakage in the macroporous walls appears after the urea treatment. However, widespread skeletal 3DOM framework was maintained. Fig. 1E and F shows the SEM images of NP TiO<sub>2</sub> and N-NP TiO<sub>2</sub> respectively. Comparing Fig. 1F with E, we can see that the nitrogen-doping process does not change the morphology of NP TiO<sub>2</sub>.

Fig. 2 shows the TG and DTG curves of the as-made 3DOM TiO<sub>2</sub> before calcination. A small weight loss (9 wt%) can be observed below 228 °C, which could be related to the removal of adsorbed ethanol and water. In the temperature range of 228–400 °C, a significant weight loss (67 wt%) can be clearly seen, which could be attributed to the removal of PMMA templates. When temperature is higher than 400 °C, no weight loss was observed, indicating that the PMMA template was completely removed.

Fig. 3 shows the EDX results for N-3DOM TiO<sub>2</sub>. It confirms the presence of N in the N-3DOM TiO<sub>2</sub> sample with a 16.31% N atomic content. In addition to the existence of Ti,

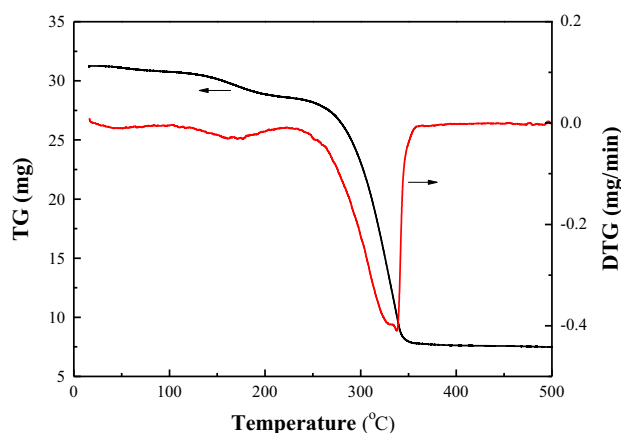


Fig. 2. Thermogravimetric (TG)/derivative thermogravimetric (DTG) curves of the as-made 3DOM TiO<sub>2</sub> sample before calcination.

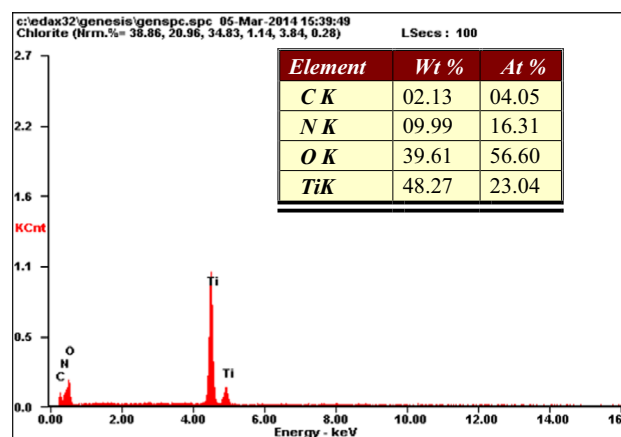


Fig. 3. EDX analysis of N-3DOM TiO<sub>2</sub>.

O and N, a small amount of C (atomic percent of 4.05%) was also detected. As discussed above, after calcination at 500 °C for 5 h, the PMMA template has been completely removed, so the small amount of C could be attributed to carbonization of the conducting resin under high voltage in the SEM test.

Fig. 4 shows the XRD patterns of the four TiO<sub>2</sub> samples. Very narrow and sharp main peaks of as-obtained samples can be observed in all patterns, indicating that all TiO<sub>2</sub> samples have higher crystalline structure. The XRD patterns of all TiO<sub>2</sub> samples show peaks at 25.3°, 37.8°, 48.0°, 55.1°, and 62.7°, which corresponds well to the main characteristic diffraction peaks of anatase (101), (004), (200), (105), (211), and (204) crystal planes (JCPDS Card no. 01-071-1166), indicating the formation of anatase phase for all samples. The calcination process not only removed the hard template, but also made the formation of anatase phase. No additional peaks such as N–O and Ti–N appeared in the pattern of N-3DOM TiO<sub>2</sub> and N-NP TiO<sub>2</sub>, which is in accordance with other nitrogen-doped TiO<sub>2</sub> reported previously [26,29].

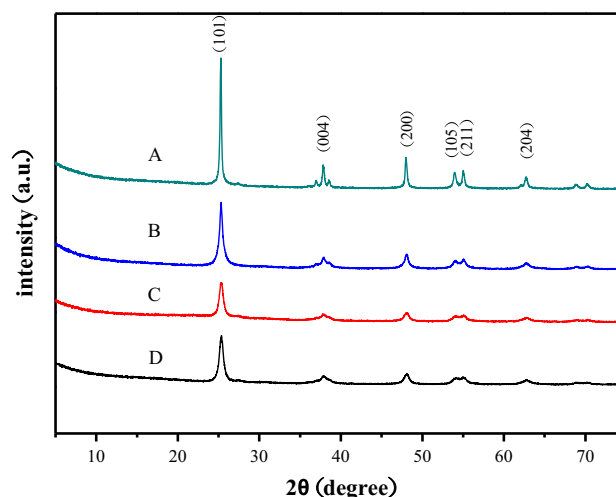


Fig. 4. X-ray diffraction patterns of (A) 3DOM TiO<sub>2</sub>; (B) N-3DOM TiO<sub>2</sub>; (C) N-NP TiO<sub>2</sub> and (D) NP TiO<sub>2</sub>.

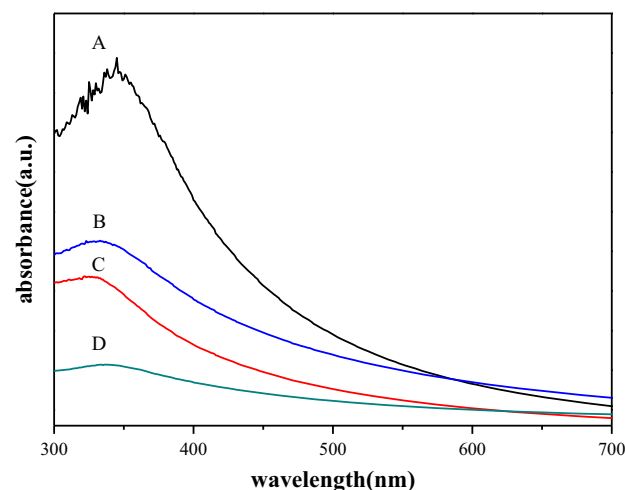


Fig. 5. UV-visible absorption spectra of (A) N-3DOM TiO<sub>2</sub>; (B) N-NP TiO<sub>2</sub> (C) 3DOM TiO<sub>2</sub> and (D) NP TiO<sub>2</sub>.

Fig. 5 shows the UV–visible absorption spectrum of 3DOM TiO<sub>2</sub> and N-3DOM TiO<sub>2</sub>, including the data for NP TiO<sub>2</sub> and N-NP TiO<sub>2</sub> sample, used here as references. As shown in Fig. 5, the order of UV–visible absorption capability for the as-prepared samples is N-3DOM TiO<sub>2</sub> > N-NP TiO<sub>2</sub> > 3DOM TiO<sub>2</sub> > NP TiO<sub>2</sub>, and the N-3DOM TiO<sub>2</sub> sample exhibited the largest optical absorption properties, especially in the visible light region (400–550 nm). Both nitrogen-doped samples (N-NP TiO<sub>2</sub> and N-3DOM TiO<sub>2</sub>) exhibited a higher optical absorption capability than the undoped TiO<sub>2</sub> samples (NP TiO<sub>2</sub> and 3DOM TiO<sub>2</sub>). Based on the above discussion, we conclude that N doping with urea is an effective method to enhance the visible light absorption property of TiO<sub>2</sub>. This enhancement could be attributed to the incorporation of N atom into the lattice of TiO<sub>2</sub>, which can induce the band gap narrowing and cause the red-shift absorption threshold of TiO<sub>2</sub>. In addition, both TiO<sub>2</sub> samples with 3DOM structure (3DOM TiO<sub>2</sub> and N-3DOM TiO<sub>2</sub>) exhibited better UV–visible absorption performance than their corresponding TiO<sub>2</sub> particle samples (NP TiO<sub>2</sub> and N-NP TiO<sub>2</sub>). This phenomenon could be ascribed to the slow photons generated by the 3DOM structure [7,8]. Slow photons generated in photonic structures such as 3DOM structure could increase the path length of the light, as the group velocity of light at the edge of these wavelengths decreases remarkably. And it has been reported that increasing the path length of light can enhance the light absorption of a material and improve its photoreaction efficiency [30].

### 3.2. Photocatalytic testing

The photocatalytic performance of 3DOM TiO<sub>2</sub>, N-3DOM TiO<sub>2</sub>, NP TiO<sub>2</sub> and N-NP TiO<sub>2</sub> was investigated by degradation of MO under UV–visible light and visible light respectively. As shown in Fig. 6, under UV–visible light, N-3DOM TiO<sub>2</sub> exhibits the highest photocatalytic activity, and the order of photocatalytic efficiency for the as-prepared samples is N-3DOM TiO<sub>2</sub> > N-NP TiO<sub>2</sub> > 3DOM TiO<sub>2</sub> > NP TiO<sub>2</sub>, which corresponds well with the samples' UV–visible absorption properties mentioned above.

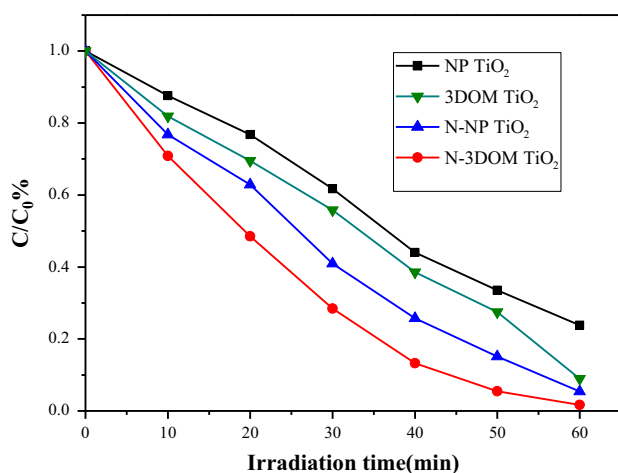


Fig. 6. Photocatalytic degradation of methyl orange (MO) over N-3DOM TiO<sub>2</sub>, 3DOM TiO<sub>2</sub>, N-NP TiO<sub>2</sub> and NP TiO<sub>2</sub> under UV–visible light.

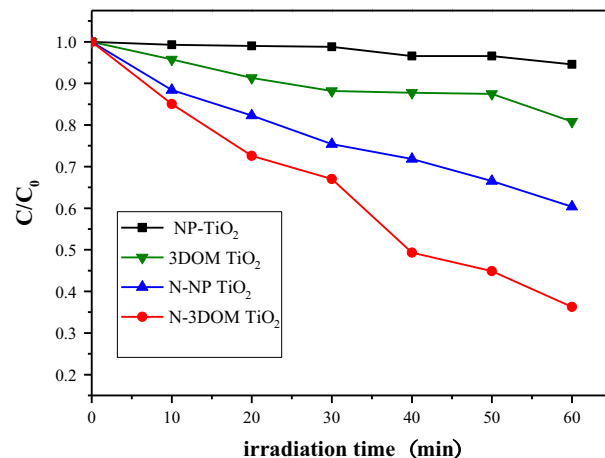


Fig. 7. Photocatalytic degradation of methyl orange (MO) over N-3DOM TiO<sub>2</sub>, 3DOM TiO<sub>2</sub>, N-NP TiO<sub>2</sub> and NP TiO<sub>2</sub> under visible light.

These results illustrate that 3DOM structure and N doping of the 3DOM structure favorably improves the photocatalytic activity of TiO<sub>2</sub>.

Fig. 7 shows the photocatalytic decomposition of MO solution over the four TiO<sub>2</sub> samples under visible light. Also N-3DOM TiO<sub>2</sub> exhibits the highest photocatalytic activity, and the order of photocatalytic efficiency for the TiO<sub>2</sub> samples is N-3DOM TiO<sub>2</sub> > N-NP TiO<sub>2</sub> > 3DOM TiO<sub>2</sub> > NP TiO<sub>2</sub>, which is in accordance with the sample's photodegradation efficiency under UV–visible light and the samples' visible light absorption properties (400–550 nm). This result confirms that N-3DOM TiO<sub>2</sub> can be activated not only by UV light but also by visible light.

It is well accepted that photocatalytic degradation of organic pollutants such as MO in an aqueous suspension follows Langmuir–Hinshelwood model [17,29]:

$$-dC/dt = K_r K_a C / (1 + K_a C) \quad (1)$$

where  $(-dC/dt)$  is the degradation rate of MO,  $C$  is the MO concentration in the solution,  $t$  is reaction time,  $K_r$  is a reaction rate constant, and  $K_a$  is the adsorption coefficient of the reactant. When the value of  $C$  is very small,  $K_a C$  is negligible. As a consequence, Eq. (1) can be described with first-order kinetics. Setting Eq. (1) under the initial conditions of the photocatalytic degradation process, that is,  $t=0$  and  $C=C_0$ , it can be described as follows:

$$\ln(C_0/C) = K_{app} t \quad (2)$$

In Eq. (2),  $K_{app}$  is the apparent rate constant. With this constant, we are able to evaluate the samples' photocatalytic activity without considering the previous adsorption period in the dark and the concentration of MO remaining in the solution. As a result, it was chosen as the basic parameter to evaluate the kinetics of different photocatalytic reactions. The dependences of the experimental and modeled values of  $\ln(C_0/C)$  on irradiation time under UV–visible light and visible light are given in Figs. 8 and 9 respectively.  $K_{app}$  are the slopes of the lines. From these figures we conclude that

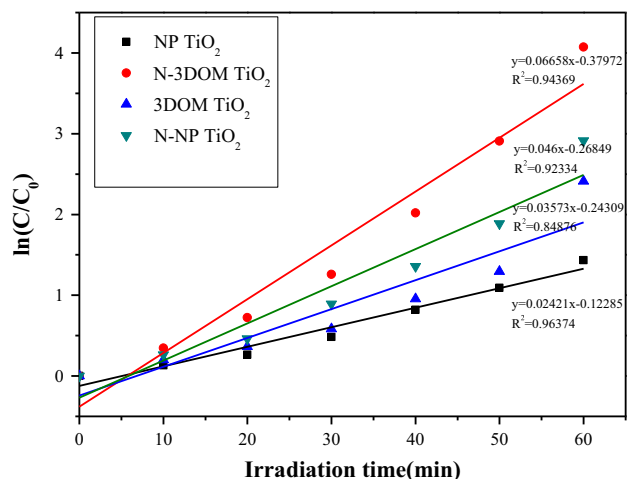


Fig. 8. Comparison of first-order degradation rates of MO for N-3DOM TiO<sub>2</sub>, 3DOM TiO<sub>2</sub>, N-NP TiO<sub>2</sub> and NP TiO<sub>2</sub> under UV-visible light.

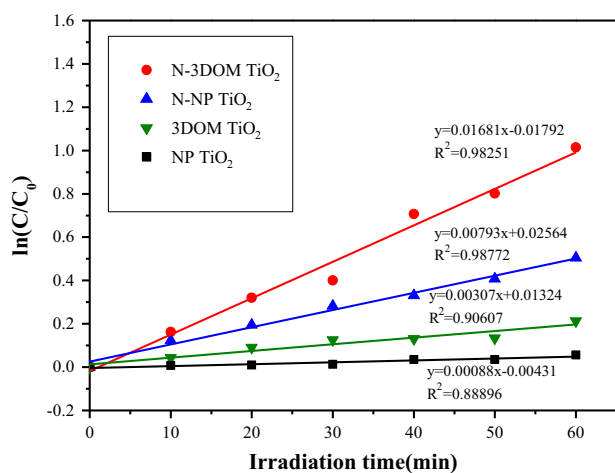


Fig. 9. Comparison of first-order degradation rates of MO for N-3DOM TiO<sub>2</sub>, 3DOM TiO<sub>2</sub>, N-NP TiO<sub>2</sub> and NP TiO<sub>2</sub> under visible light.

both N-3DOM TiO<sub>2</sub> and 3DOM TiO<sub>2</sub>, which possess 3DOM structure, exhibit stronger photocatalytic activity for degradation of MO under UV-visible light and visible light irradiation than that of NP TiO<sub>2</sub>. Especially N-3DOM TiO<sub>2</sub> which performed 2.75 times and 19.1 times better than NP TiO<sub>2</sub> under UV-visible light and visible light respectively, based on their respective  $K_{app}$  values.

The better photocatalytic activity of N-3DOM TiO<sub>2</sub> and 3DOM TiO<sub>2</sub> compared to NP TiO<sub>2</sub> is attributed to the following factors. The 3DOM structure promotes reactant diffusion [17] access to the surface active sites. The 3DOM structure also generates slow photons which can increase the path length of light, thus enhancing its light absorption and improving its photoreaction efficiency [7,8]. Furthermore, the band gap narrowing of 3DOM TiO<sub>2</sub> by N doping leads to the enhancement of visible light absorption efficiency, as confirmed by the samples' UV-visible absorption spectra. Thus, N-doped TiO<sub>2</sub> with 3DOM structure can be activated not only by UV light but also by visible light. More electrons and holes can be generated by the modified TiO<sub>2</sub> to more effectively participate in the

photocatalytic redox reactions. As a result, TiO<sub>2</sub>'s photocatalytic activity was significantly improved with N doping and 3DOM structure.

#### 4. Conclusion

We have synthesized three-dimensionally ordered macroporous titanium dioxide (3DOM TiO<sub>2</sub>) with the colloidal crystal template method using poly-(methyl methacrylate) (PMMA) as a hard template. N doped 3DOM TiO<sub>2</sub> (N-3DOM TiO<sub>2</sub>) was also prepared by a facile impregnation method. Both 3DOM TiO<sub>2</sub> and N-3DOM TiO<sub>2</sub> demonstrate enhanced photodegradation efficiency under UV-visible light and visible light, which is attributed to the impact of N doping and the 3DOM structure. Our work suggests that the coupling of 3DOM structure with nitrogen doping can significantly improve the photocatalytic activity of TiO<sub>2</sub> materials, which could have great application potentials in the fields of environmental protection, solar cell devices, and so on.

#### Acknowledgments

This work is financially supported by the Shandong Province Natural Science Foundation of China (Grant no. ZR2011BQ014), Key Joint Foundation of PetroChina and National Natural Science Foundation of China (Grant no. U1362202), National Natural Science Foundation of China (Grant no. 21303130), and Fundamental Research Funds for the Central Universities (Grant no. 12CX04093A). The authors also thank Dr. Changhua An and Professor Mark J. Rood for their kind helps.

#### References

- [1] J.J. Chiu, D.J. Pine, S.T. Bishop, B.F. Chmelka, Friedel-Crafts alkylation properties of aluminosilica SBA-15 meso/macroporous monoliths and mesoporous powders, *J. Catal.* 221 (2004) 400–412.
- [2] K. Na, C. Jo, J. Kim, K. Cho, J. Jung, Y. Seo, R.J. Messinger, B. F. Chmelka, R. Ryoo, Directing zeolite structures into hierarchically nanoporous architectures, *Science* 333 (2011) 328–332.
- [3] P. Yang, T. Deng, D. Zhao, P. Feng, D. Pine, B.F. Chmelka, G. M. Whitesides, G.D. Stucky, Hierarchically ordered oxides, *Science* 282 (1998) 2244–2246.
- [4] L.Z. Fan, Y.S. Hu, J. Maier, P. Adelhelm, B. Smarsly, M. Antonietti, High electroactivity of polyaniline in supercapacitors by using a hierarchically porous carbon monolith as a support, *Adv. Funct. Mater.* 17 (2007) 3083–3087.
- [5] A. Stein, R.C. Schroden, Colloidal crystal templating of three-dimensionally ordered macroporous solids: materials for photonics and beyond, *Curr. Opin. Solid State Mater. Sci.* 5 (2001) 553–564.
- [6] A. Stein, F. Li, N.R. Denny, Morphological control in colloidal crystal templating of inverse opals, hierarchical structures, and shaped particles, *Chem. Mater.* 20 (2007) 649–666.
- [7] M. Wu, Y. Li, Z. Deng, B.-L. Su, Three-dimensionally ordered macroporous titania with structural and photonic effects for enhanced photocatalytic efficiency, *ChemSusChem* 4 (2011) 1481–1488.
- [8] J.I.L. Chen, G. von Freymann, S.Y. Choi, V. Kitaev, G.A. Ozin, Amplified photochemistry with slow photons, *Adv. Mater.* 18 (2006) 1915–1919.

- [9] O.D. Velev, E.W. Kaler, Structured porous materials via colloidal crystal templating: from inorganic oxides to metals, *Adv. Mater.* 12 (2000) 531–534.
- [10] J.W. Galusha, C.-K. Tsung, G.D. Stucky, M.H. Bartl, Optimizing sol–gel infiltration and processing methods for the fabrication of high-quality planar titania inverse opals, *Chem. Mater.* 20 (2008) 4925–4930.
- [11] M.A. Al-Daous, A. Stein, Preparation and catalytic evaluation of macroporous crystalline sulfated zirconium dioxide templated with colloidal crystals, *Chem. Mater.* 15 (2003) 2638–2645.
- [12] R.C. Schrodin, C.F. Blanford, B.J. Melde, B.J.S. Johnson, A. Stein, Direct synthesis of ordered macroporous silica materials functionalized with polyoxometalate clusters, *Chem. Mater.* 13 (2001) 1074–1081.
- [13] D. Han, X. Li, L. Zhang, Y. Wang, Z. Yan, S. Liu, Hierarchically ordered meso/macroporous  $\gamma$ -alumina for enhanced hydrodesulfurization performance, *Microporous Mesoporous Mater.* 158 (2012) 1–6.
- [14] L.I. Halaoui, N.M. Abrams, T.E. Mallouk, Increasing the conversion efficiency of dye-sensitized TiO<sub>2</sub> photoelectrochemical cells by coupling to photonic crystals, *J. Phys. Chem. B* 109 (2005) 6334–6342.
- [15] J. Du, X. Lai, J. Halpert, Y. Yang, D. Wang, Formation of efficient dye-sensitized solar cells by introducing an interfacial layer of hierarchically ordered macro-mesoporous TiO<sub>2</sub> film, *Sci. China Chem.* 54 (2011) 930–935.
- [16] G. Yang, B. Yang, T. Xiao, Z. Yan, One-step solvothermal synthesis of hierarchically porous nanostructured CdS/TiO<sub>2</sub> heterojunction with higher visible light photocatalytic activity, *Appl. Surf. Sci.* 283 (2013) 402–410.
- [17] M. Srinivasan, T. White, Degradation of methylene blue by three-dimensionally ordered macroporous titania, *Environ. Sci. Technol.* 41 (2007) 4405–4409.
- [18] A. Fujishima, K. Honda, Electrochemical photolysis of water at a semiconductor electrode, *Nature* 238 (1972) 37–38.
- [19] A. Kudo, K. Omori, H. Kato, A novel aqueous process for preparation of crystal form-controlled and highly crystalline BiVO<sub>4</sub> powder from layered vanadates at room temperature and its photocatalytic and photophysical properties, *J. Am. Chem. Soc.* 121 (1999) 11459–11467.
- [20] Z. He, W. Que, Y. He, J. Hu, J. Chen, H.M. Asif Javed, Electrochemical behavior and photocatalytic performance of nitrogen-doped TiO<sub>2</sub> nanotubes arrays powders prepared by combining anodization with solvothermal process, *Ceram. Int.* 39 (2013) 5545–5552.
- [21] G. Yang, T. Wang, B. Yang, Z. Yan, S. Ding, T. Xiao, Enhanced visible-light activity of F-N co-doped TiO<sub>2</sub> nanocrystals via nonmetal impurity, Ti<sup>3+</sup> ions and oxygen vacancies, *Appl. Surf. Sci.* 287 (2013) 135–142.
- [22] Y. Liu, J. Liu, Y. Lin, Y. Zhang, Y. Wei, Simple fabrication and photocatalytic activity of S-doped TiO<sub>2</sub> under low power LED visible light irradiation, *Ceram. Int.* 35 (2009) 3061–3065.
- [23] G. Wu, T. Nishikawa, B. Ohtani, A. Chen, Synthesis and characterization of carbon-doped TiO<sub>2</sub> nanostructures with enhanced visible light response, *Chem. Mater.* 19 (2007) 4530–4537.
- [24] G. Yang, T. Xiao, J. Sloan, G. Li, Z. Yan, Low-temperature synthesis of visible-light active fluorine/sulfur Co-doped mesoporous TiO<sub>2</sub> microspheres, *Chem. Eur. J.* 17 (2011) 1096–1100.
- [25] G. Yang, Z. Jiang, H. Shi, M.O. Jones, T. Xiao, P.P. Edwards, Z. Yan, Study on the photocatalysis of F–S co-doped TiO<sub>2</sub> prepared using solvothermal method, *Appl. Catal. B* 96 (2010) 458–465.
- [26] G. Yang, Z. Jiang, H. Shi, T. Xiao, Z. Yan, Preparation of highly visible-light active N-doped TiO<sub>2</sub> photocatalyst, *J. Mater. Chem.* 20 (2010) 5301–5309.
- [27] B.T. Holland, C.F. Blanford, A. Stein, Synthesis of macroporous minerals with highly ordered three-dimensional arrays of spheroidal voids, *Science* 281 (1998) 538–540.
- [28] B.T. Holland, C.F. Blanford, T. Do, A. Stein, Synthesis of highly ordered, three-dimensional, macroporous structures of amorphous or crystalline inorganic oxides, phosphates, and hybrid composites, *Chem. Mater.* 11 (1999) 795–805.
- [29] Y. Ao, J. Xu, D. Fu, C. Yuan, A simple method to prepare N-doped titania hollow spheres with high photocatalytic activity under visible light, *J. Hazard. Mater.* 167 (2009) 413–417.
- [30] P.G. O'Brien, N.P. Kherani, S. Zukotynski, G.A. Ozin, E. Vekris, N. Tetreault, A. Chutinan, S. John, A. Mihi, H. Míguez, Enhanced photoconductivity in thin-film semiconductors optically coupled to photonic crystals, *Adv. Mater.* 19 (2007) 4177–4182.